

Low-loss silica-on-silicon two-dimensional Fabry–Perot cavity based on holographic Bragg reflectors

Christoph M. Greiner, Dmitri Iazikov, and Thomas W. Mossberg

LightSmyth Technologies, Inc., Suite 250, 860 West Park Street, Eugene, Oregon 97041

Received August 27, 2004

We report on the demonstration of an integrated slab-waveguide-based concentric Fabry–Perot resonator that employs holographic Bragg reflectors as cavity mirrors. The cavity, produced in a low-loss silica-on-silicon slab waveguide by high-fidelity deep-ultraviolet photolithographic fabrication, exhibits a reflectivity-limited Q factor of approximately 10^5 . Increasing the mirror's reflectivity will provide Q values similar to those of silica-based ring resonators, whereas the folded Fabry–Perot resonator design allows access to a substantially larger free spectral range by cavity shortening. © 2005 Optical Society of America

OCIS codes: 130.3120, 230.5750.

Optical resonators based on planar lightwave circuits have recently attracted much attention as the basis of a range of spectral filtering applications including add–drop channel filters,^{1–3} wavelength-division multiplexers–demultiplexers,⁴ dispersion compensators,⁵ sensors, and tunable filters and modulators.^{6,7} We report on a different approach to integrated resonator design that employs silica-on-silicon-based holographic Bragg reflectors⁸ (HBRs) and a concentric Fabry–Perot architecture. HBRs are computer-generated holographic refractive-index structures created throughout regions of slab waveguides by deep ultraviolet projection photolithography. They have recently been demonstrated as engines for coarse,⁹ dense,¹⁰ and code-division¹¹ multiplexing as well as general filtering applications including spectral comparison.¹²

Previous research with PLC-based cavities has included Fabry–Perot^{6,7} as well as ring resonator^{1–5,13–15} architectures. Use of the former geometry has been restricted to one-dimensional ridge waveguide segments sandwiched between dielectric or Bragg reflectors, an approach that is substantially different from the fully two dimensional slab-waveguide-based approach pursued here. Ring resonators have been a focus of intense photonics research for a long time and have been achieved by use of both high- and low-refractive-index materials. The latter approach provides large free-spectral ranges (FSRs), yet high propagation losses have impeded practical device implementation. Q factors of 10^6 were demonstrated in low-index-contrast silica-based ring resonators,^{13,14} but FSRs demonstrated to date are limited to less than 100 GHz (Ref. 15) owing to constraints on acceptable bending losses. Additional drawbacks of the ring resonator architecture are the typically polarization-dependent waveguide-to-ring-resonator coupling and ring propagation constants^{1,16} as well as the general lack of design flexibility in wavelength tailoring of the coupling constant. Recent advances in this area show promise for resolution of these issues.¹⁷

Because of its folded Fabry–Perot geometry the present approach to resonator design allows access to

FSRs that substantially exceed those of silica-based ring resonators. Furthermore, the low-loss silica platform makes HBR-based resonators fully consistent with similar Q factors. HBR cavity mirrors are physically distinct elements whose reflective properties can be broadly tailored in a straightforward fashion,⁸ thus affecting desired cavity spectral properties.

Figure 1(a) is a schematic top view of the slab-waveguide-based asymmetric concave–convex concentric cavity. The cavity consists of two 266- μm -long HBRs that function as cavity mirrors. The 4-mm spacing between mirrors yields a FSR of ~ 26 GHz. The circular contour HBR mirrors, with radii of 3 and 7 mm, are concentric about point C. In operation, light emerges from the end of the channel input waveguide shown to the left of the cavity, expands in the open slab region at the left, and subsequently, if it is resonant with one of its modes, builds up in the resonator. A second channel waveguide behind the right-hand cavity mirror can be used to monitor the cavity transmission. Input and transmission collecting channel waveguides have a design opening

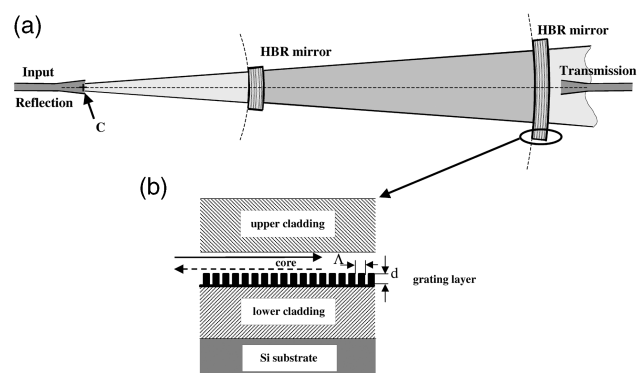


Fig. 1. Integrated cavity. (a) Top view, showing the cavity comprising two HBRs functioning as cavity mirrors and input and output channel waveguides. The HBR mirrors are concentric about center of curvature C. (b) Cross-sectional HBR view: d , grating height; Λ , grating period.

of 12.7 μm and 20 μm , respectively, which is adiabatically increased from 6 μm at the die edge via a 0.5 mm-long taper. The cavity's footprint (excluding the access waveguides) is a mere 8.5 mm².

Figure 1(b) is a partial cross-sectional view of one of the cavity's HBRs. In the HBR region the silica slab waveguide consists of a doped dual-layer core and bilateral 15- μm -thick cladding layers. The dual-layer core comprises a 1- μm -thick grating layer that has a +3% refractive-index contrast relative to the cladding and a 1.6- μm -thick core layer with a +1% refractive-index contrast relative to the cladding. Depicted at the interface between the two core sublayers are cross sections of representative lithographically scribed grating contours. The diffractive contours, with depth $d \approx 850$ nm, consist of trenches etched into the grating layer and filled with material of the upper core sublayer. The HBR operates in first diffractive order with a contour spacing, Λ , of ~ 500 nm, i.e., one half of the in-medium wavelength of resonant light. Outside the grating region the thicknesses of the upper core and grating layers are 2 μm and 150 nm, respectively (the same etch that creates the HBR etches away most of the grating layer outside the cavity and in its interior). The cavity was fabricated on a deep-ultraviolet optical stepper employing a laser-written reticle and standard etching, deposition, and annealing processes.

Figure 2(a) shows the spectral profile of the cavity measured in retroreflection back through the input channel waveguide [to the left in Fig. 1(a)] and a TM-polarized tunable narrow-linewidth laser. The periodic dips in the reflection spectrum correspond to the cavity transmission modes. The overall slow sinc-functionlike modulation of the observed spectrum is caused by the sinc-function spectral transfer function of the unapodized HBR cavity mirrors [with an estimated primary passband (FWHM) of ~ 3.9 nm]. Figure 2(b) shows a portion of the cavity's transmission spectrum. The cavity's FSR and bandpass were determined to be 25.9 (0.04) and 2.8 (0.2) GHz, where the numbers in parentheses are error limits, yielding a finesse of 9.2 (0.6). The choice, in Fig. 2, of showing the cavity's spectral properties for TM rather than TE-polarized input light was an arbitrary one. For TE-polarized light, the bandpass and the finesse were found, respectively, to be 2.56 (0.14) GHz and 10.2 (0.6). Error bars represent standard deviations over multiple observed cavity resonances. The TE-finesse value is higher than for TM polarization owing to a slightly higher mirror reflectivity for TE polarization, as we detail in what follows. The absolute intrinsic insertion loss of the cavity, measured off cavity resonance in retroreflection for TM [TE] polarization, was 0.3 (0.1) dB [0.4 (0.1) dB]. This value excludes fiber-to-die coupling but includes channel-to-slab internal coupling. The insertion loss difference for the two polarization states, commonly referred to as polarization-dependent loss, was found to be 0.1 (0.2) dB.

It is instructive to compare the measured cavity performance with the theoretically expected behavior and specifically to attempt to quantify cavity loss. Examples of potential sources of loss are scattering

and (or) absorption within the HBRs or in the cavity's internal waveguide region and diffractive losses from the conditionally stable cavity. Furthermore, a fully two-dimensional cavity as considered here is highly sensitive to, and is thus a powerful diagnostic tool for, fabrication errors, such as effective index inhomogeneities of the interior slab waveguide and inaccurate lithographic rendition of the HBR contours. Such errors affect the transverse spatial coherence of the intracavity field and limit finesse. The importance of transverse spatial coherence makes the present two-dimensional resonator substantially different from previously demonstrated one-dimensional Fabry–Perot cavities.^{6,7} Interestingly, we have found that fabrication errors that affect the transverse wave-front coherence are so small that measured cavity performance correlates essentially perfectly with a one-dimensional cavity with reflectivity-limited finesse.

Based on measurement of other HBRs fabricated simultaneously with the Fabry–Perot cavity of Fig. 1, we have determined the extinction length ($1/e$ distance of the electric field) of the HBRs employed to be 375 (10) μm for TM polarization [355 (10) μm for TE polarization]. Based on these values, we estimate the peak reflectivity for each 266- μm -long HBR cavity mirror to be 68.6 (1.8)% [71.8 (1.7)%] and a cavity finesse of 8.3 (0.6) [9.4 (0.7)] for TM- (TE-) polarized input light, respectively. The relatively low mirror reflectivity of this initial design was chosen because losses were initially unknown and because resonator characterization by use of cavity transmission produces largest signal levels when the mirror transmittance is at least

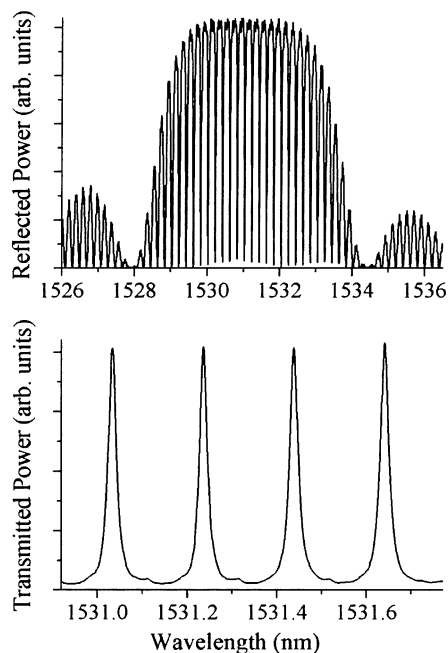


Fig. 2. (a) Cavity reflection profile. Periodic dips in the measured spectrum correspond to resonant cavity modes. The overall envelope modulation observed is due to the reflective profile of the HBR cavity mirrors (~ 3.9 -nm primary passband). (b) Transmission spectrum at the center of the HBR passband, showing cavity modes and FSR. All data shown were measured with TM polarization.

comparable with the round-trip loss. Importantly, however, comparison of theoretically derived with measured finesse values indicates that the cavity loss is not only small but is actually consistent (within experimental error) with zero loss. The observed finesse allows us to set an upper limit on the round-trip cavity field loss (HBRs and internal slab waveguide region) equal to 1.2% [1.8%] for TM [TE] polarization. Our results indicate that the demonstrated cavity Q factor of almost 10^5 is limited only by the relatively low mirror reflectivity. Mirror reflectivity may be productively increased until transmission and loss are comparable. With the upper limits on loss found here it is believed that a cavity Q of 10^6 or more may be readily obtainable to provide Q -value performance similar to that offered by silica-based ring resonators.^{13,14}

It is well known from optical resonator theory¹⁸ that phase errors that affect transverse spatial coherence can constrain the maximally achievable finesse. Specifically, an optical path-length variation of λ/M across a cavity's aperture implies a (mirror-figure-limited) finesse of $M/2$. Consequently, our finesse result indicates that in this device the phase errors that were due to inaccurate lithographic rendition or refractive-index variations are limited to only $\sim\lambda/20$ or less. The profound ultrahigh fabrication fidelity testifies to the power of the deep-ultraviolet photolithographic fabrication process and the uniformity of the slab-waveguide environment.

In the present device a weak polarization dependence of the cavity transmission spectrum was measured. Specifically, TE-polarized input light was found to be resonant with the cavity at wavelengths that were redshifted by ~ 80 pm from the TM response. Preliminary results with HBR test structures indicate that tuning of HBR birefringence properties by structural and compositional tailoring of the grating layer morphology is possible. Such tuning provides a pathway to compensate for differences in propagation constants found in the cavity interior, thus yielding a polarization-insensitive spectral response. Note that, in the limit of low loss, an inherent advantage of the present cavity design, which employs equally reflective mirrors, is that any polarization dependence of the mirror's reflectivity will affect only the width of the cavity resonances but not their peak transmission. In the limit of high reflectivity, the present cavity type exhibits not an appreciable true polarization-dependent loss but rather a (small) difference in the reflection bandwidth, an effect that is often irrelevant to resonator operation.

In summary, an integrated concentric Fabry–Perot cavity based on holographic Bragg reflectors has been demonstrated. HBRs make possible slab-waveguide analogs of general three-dimensional discrete mirror-based resonators, including those with standing or traveling wave modes. Enabled cavities include stable single-mode designs and more-complex mode-degenerate varieties such as the confocal resonator. The present results indicate that Q values comparable with those of integrated silica ring resonators can be achieved. The reflective geometry of the HBR-based

cavities means that large FSRs (which are difficult to achieve in low-index contrast ring resonators) can easily be achieved. Reflection bands of the physically distinct HBR-based cavity mirrors can be tailored with previously demonstrated apodization approaches.⁸ This permits, for example, unambiguous filtering operation when mirror passbands are limited to one or a few spectral ranges in width. HBR-based integrated cavities may be used as all-pass phase-only filters for dispersion compensation.

The authors thank B. Brainard, Z. Dong, N. Gopinathan, D. Nakamoto, S. Theedki, and A. Vaidyanathan for sharing their fabrication expertise. C. M. Greiner's e-mail address is cgreiner@lightsmyth.com.

References

1. M. K. Chin, C. Youtsey, W. Zhao, T. Pierson, Z. Ren, S. L. Wu, L. Wang, Y. G. Zhao, and S. T. Ho, *IEEE Photon. Technol. Lett.* **11**, 1620 (1999).
2. B. E. Little, J. S. Foresi, G. Steinmeyer, E. R. Thoen, S. T. Chu, H. A. Haus, E. P. Ippen, L. C. Kimmerling, and W. Greene, *IEEE Photon. Technol. Lett.* **10**, 549 (1998).
3. D. Rafizadeh, J. P. Zhang, S. C. Hagness, A. Taflove, K. A. Stair, and S. T. Ho, *Opt. Lett.* **22**, 1244 (1997).
4. S. T. Chu, B. E. Little, W. Pan, T. Kaneko, S. Sato, and Y. Kokubun, *IEEE Photon. Technol. Lett.* **11**, 691 (1999).
5. C. K. Madsen and G. Lenz, *IEEE Photon. Technol. Lett.* **10**, 994 (1998).
6. H. K. Tsang, M. W. K. Mak, L. Y. Chan, J. B. D. Soole, C. Youtsey, and I. Adesida, *J. Lightwave Technol.* **17**, 1890 (1999).
7. C. Angulo Barrios, V. R. Almeida, R. R. Panepucci, B. S. Schmidt, and M. Lipson, *IEEE Photon. Technol. Lett.* **16**, 506 (2004).
8. C. Greiner, D. Iazikov, and T. W. Mossberg, *J. Lightwave Technol.* **22**, 136 (2004).
9. D. Iazikov, C. Greiner, and T. W. Mossberg, *J. Lightwave Technol.* **22**, 1402 (2004).
10. C. Greiner, D. Iazikov, and T. W. Mossberg, *Appl. Opt.* **43**, 4575 (2004).
11. Y.-K. Huang, V. Baby, P. R. Prucnal, C. Greiner, D. Iazikov, and T. W. Mossberg, "Integrated holographic encoder/decoder for wavelength-hopping/time-spreading optical CDMA," submitted to *Photon. Technol. Lett.*
12. T. W. Mossberg, D. Iazikov, and C. Greiner, *J. Opt. Soc. Am. A* **21**, 1088 (2004).
13. T. Kominato, Y. Ohmori, N. Takato, H. Okazaki, and M. Yasu, *J. Lightwave Technol.* **10**, 1781 (1992).
14. S. Suzuki, K. Shuto, and Y. Hibino, *IEEE Photon. Technol. Lett.* **4**, 1256 (1992).
15. G. Bourdon, G. Alibert, A. Beguin, B. Bellman, and E. Guiot, *IEEE Photon. Technol. Lett.* **15**, 994 (2003).
16. M. K. Chin, *Opt. Express* **11**, 1724 (2003), <http://www.opticsexpress.org>.
17. B. Little, S. T. Chu, P. P. Absil, J. V. Hryniewicz, F. G. Johnson, F. Seiferth, D. Gill, V. Van, O. King, and M. Trakalo, *IEEE Photon. Technol. Lett.* **16**, 2263 (2004).
18. R. D. Guenther, *Modern Optics* (Wiley, New York, 1990).